Dipole and nondipole photoionization of molecular hydrogen

B. Zimmermann, V. McKoy, S. H. Southworth, E. P. Kanter, B. Krässig, and R. Wehlitz

Phys. Rev. A **91**, 053410 — Published 15 May 2015

DOI: 10.1103/PhysRevA.91.053410

Dipole and nondipole photoionization of molecular hydrogen

B. Zimmermann* and V. McKoy

A. A. Noyes Laboratory of Chemical Physics,

California Institute of Technology, Pasadena, California 91125

S. H. Southworth, E. P. Kanter, and B. Krässig

Argonne National Laboratory, Argonne, Illinois 60439

R. Wehlitz

Synchrotron Radiation Center, University of

Wisconsin–Madison, Stoughton, Wisconsin 53589

Abstract

We describe a new theoretical approach to molecular photoionization that includes first-order corrections to the dipole approximation. The theoretical formalism is presented and applied to photoionization of H_2 over the 20–180 eV photon energy range. The angle-integrated cross section σ, the electric dipole anisotropy parameter β_e, the molecular alignment anisotropy parameter β_m, and the first-order nondipole asymmetry parameters γ and δ were calculated within the single-channel, static-exchange approximation. The calculated parameters are compared with previous measurements of σ and β_m and new measurements of β_e and $\gamma + 3\delta$. The dipole and nondipole angular distribution parameters were determined simultaneously using an efficient, multi-angle measurement technique. Good overall agreement is observed between the magnitudes and spectral variations of the calculated and measured parameters. The nondipole asymmetries of He 1s and Ne 2p photoelectrons were also measured in the course of this work.

PACS numbers: 33.80.Eh, 33.60.+q

*Present address: Wolfram Research, Champaign, Illinois 61820

I. INTRODUCTION

Photoionization of H_2 is of fundamental interest and is an important process in astronomical environments [1, 2]. H_2 is a two-electron system, like atomic He, but with the additional complexities of nonspherical structure and nuclear degrees of freedom. Several aspects of molecular photoionization have been studied in H_2, beginning with the total and dissociative photoionization cross sections [2–4]. Other aspects include ion–pair formation [5], double photoionization [6], vibrational autoionization [7], rotational and vibrational structure in the photoelectron spectrum [8, 9], resonant photoionization involving doubly excited states [10–12], and the photoelectron [13] and photoion [6, 14] angular distributions. Other research includes a study of competition between photodissociation and photoionization [15], nonperturbative time-dependent calculations of ionization by femtosecond xuv laser pulses [16], strong–field infrared laser ionization [17], and symmetry breaking in dissociative photoionization [18]. Those processes can be understood and treated within the dipole approximation to the photon-electron interaction. Here we discuss a new aspect of H_2 photoionization – *nondipole asymmetries* of photoelectron angular distributions.

Nondipole interactions produce asymmetries in photoelectron angular distributions that are neglected in the dipole approximation. A measureable effect of these interactions is to redistribute the differential photoionization cross section asymmetrically in the forward and backward directions with respect to the photon propagation vector. Early theories of the photoeffect were geared toward x-ray photoionization and large kinetic energies, and nondipole asymmetries were treated by retardation corrections in the point–Coulomb potential [19, 20]. This model neglects screening and may be inaccurate as the energy is lowered toward threshold [21–23]. Recent theories adopt the "first retardation correction" to the dipole approximation, which includes cross terms of electric dipole ($E1$) photoionization amplitudes with electric quadrupole ($E2$) and magnetic dipole ($M1$) amplitudes [21, 22, 24–26]. For photoionization of randomly oriented atoms or molecules by a linearly polarized photon beam, the differential cross section can be expressed as [24]

$$\frac{d\sigma}{d\Omega}(\theta,\phi) = \frac{\sigma}{4\pi}\left\{1 + \beta_e P_2(\cos\theta) + (\delta + \gamma\cos^2\theta)\sin\theta\cos\phi\right\}, \tag{1}$$

where σ is the angle-integrated cross section, β_e is the electric dipole anisotropy parameter, $P_2(\cos\theta) = (3\cos^2\theta - 1)/2$ is the second Legendre polynomial, and δ and γ are the first-order nondipole asymmetry parameters resulting from $E1 - E2$ and $E1 - M1$ cross terms. The

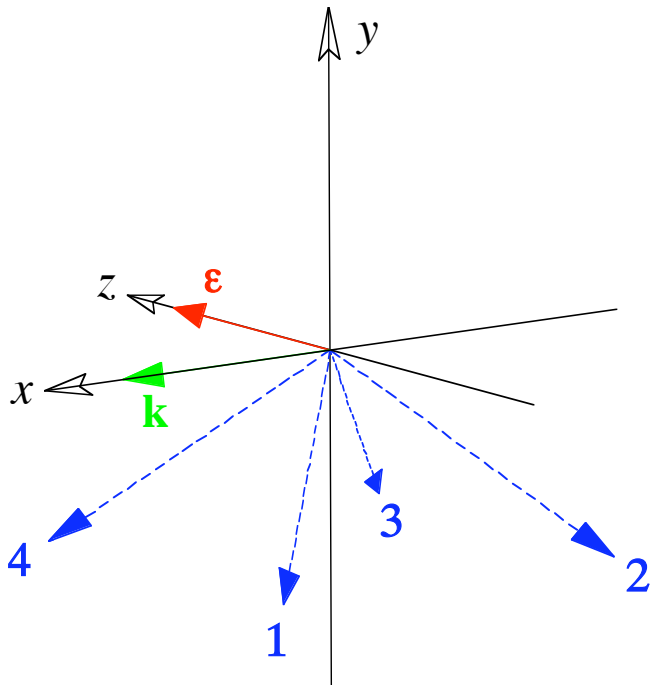

Figure 1: (Color online) The coordinate system for calculations and measurements of photoelectron angular distributions is defined by the photon propagation vector **k** along the x axis and linear polarization vector $\boldsymbol{\epsilon}$ along the z axis. The arrows labeled 1–4 represent the angular positions of the four electron analyzers used in the present work. The analyzers are positioned symmetrically around the y axis and are rotatable about that axis. See text for details.

polar and azimuthal angles θ and ϕ of the emitted photoelectrons are defined with respect to the coordinate system shown in Fig. 1 with x axis along the photon propagation vector **k** and z axis along the polarization vector $\boldsymbol{\epsilon}$. The dipole and nondipole angular distribution parameters can be determined from measurements of the photoelectron intensities with respect to **k** and $\boldsymbol{\epsilon}$ [23, 27].

Screened wavefunctions have been used to accurately calculate nondipole asymmetries of atoms over energy ranges extending from near threshold to thousands of electron volts [21–23]. Since nondipole asymmetries are generally proportional to the photon momentum or energy, relatively large asymmetries are observed for inner-shell electrons in the x-ray regime [23, 28]. However, nondipole asymmetries have also been studied in valence-shell photoionization over the ∼20–200 eV photon energy range. The accurate methods that were developed for calculations of atomic photoionization within the dipole approximation [29, 30] have been extended to calculations of nondipole asymmetries, including bound-continuum

and continuum-continuum interactions [25, 26]. Nondipole asymmetries yield new insight into photoionization dynamics such as Cooper minima and interchannel coupling [27, 31, 32].

Molecular photoionization theory is more challenging due to the nonspherical molecular potential and nuclear degrees of freedom. Only a few calculations of molecular nondipole asymmetries have been reported [33–36]. Here we describe a theory of molecular photoionization that includes $E1-E2$ and $E1-M1$ cross terms for calculations of the nondipole asymmetry parameters γ and δ in addition to the dipole parameters σ and β_e. The theory also provides calculations of the molecular anisotropy parameter β_m that describes alignment of the molecular axis in the photoionization process [14].

The theory was first applied to calculation of valence-shell nondipole asymmetries of N_2 over the 20–200 eV photon energy range that were compared with measurements in Ref. [37]. The nondipole asymmetries of the $3\sigma_g$, $1\pi_u$, and $2\sigma_u$ electrons of N_2 display different spectral variations and therefore are sensitive to the bound and continuum molecular wavefunctions. Here we describe the theoretical formalism in detail and apply it to calculations of H_2 over the 20–180 eV photon energy range. The calculated parameters are compared with existing measurements of σ and β_m and with new measurements of β_e and $\gamma+3\delta$. In comparison with previous theoretical treatments of nondipole effects in molecular photoionization, Refs. [33–36], the present work is distinguished by being both very general in its development and by employing well tested frozen-core Hartree-Fock calculational codes [38].

Section II of this paper describes the theoretical formalism and calculational methods. Section III describes the photoelectron spectrometer and measurements. Section IV compares measured and calculated photoionization parameters. Conclusions and suggestions for future research are given in section V.

II. THEORY

A. Photon states of definite angular momentum and parity

One can find a number of multipole descriptions of photons [39–41], so the description used in this article will be brief. Starting from the Rayleigh expansion, the plane wave describing a photon can be expanded using vector spherical harmonics [42] and the transverse

nature of the photon wave ($\mathbf{k}_\mathrm{p} \cdot \boldsymbol{\varepsilon} = 0$) into the multipole series [43]

$$\boldsymbol{\varepsilon}\, \exp(i\, \mathbf{k}_\mathrm{p} \cdot \mathbf{r}) = \sum_{LMx} C^x_{LM}(\hat{\mathbf{k}}_\mathrm{p})\, \mathbf{a}^x_{LM}(\mathbf{r}). \tag{2}$$

$\boldsymbol{\varepsilon}$ is the electric vector of the photon and $\hat{\mathbf{k}}_\mathrm{p}$ is the normalized photon momentum. (Throughout the paper a hat over a vector indicates that it is normalized.) L and M are the multipole angular indices and $x = 0, 1$ characterizes the parity of the multipole, i.e., $x = 0$ refers to a magnetic and $x = 1$ to an electric multipole. The radial dependence is defined using vector spherical harmonics [42] as

$$\mathbf{a}^0_{LM}(\mathbf{r}) \;=\; j_L(k_p r)\, \mathbf{Y}^L_{LM}(\hat{\mathbf{r}}) \tag{3}$$

$$\mathbf{a}^1_{LM}(\mathbf{r}) \;=\; \sqrt{\frac{L+1}{2L+1}}\, j_{L-1}(k_p r)\, \mathbf{Y}^{L-1}_{LM}(\hat{\mathbf{r}}) - \sqrt{\frac{L}{2L+1}}\, j_{L+1}(k_p r)\, \mathbf{Y}^{L+1}_{LM}(\hat{\mathbf{r}}). \tag{4}$$

$j_l(z)$ is a spherical Bessel function: $j_l(z) = \sqrt{\pi/(2z)}\, J_{l+1/2}(z)$. The polarization part is combined to

$$C^x_{LM}(\hat{\mathbf{k}}_\mathrm{p}) = 4\pi\, i^{L-x} \left(\boldsymbol{\varepsilon} \cdot \mathbf{Y}^{(x)*}_{LM}(\hat{\mathbf{k}}_\mathrm{p}) \right). \tag{5}$$

The density matrix ρ_p of the photon state is then

$$\rho_p = \sum_{\substack{L\,M\,x \\ L'M'x'}} \left| C^x_{LM}(\hat{\mathbf{k}}_\mathrm{p})\, \mathbf{a}^x_{LM}(\mathbf{r}) \right\rangle \left\langle C^{x'}_{L'M'}(\hat{\mathbf{k}}_\mathrm{p})\, \mathbf{a}^{x'}_{L'M'}(\mathbf{r}) \right|. \tag{6}$$

In the last equations vector spherical harmonics are used. They are defined as [42]

$$\mathbf{Y}^L_{JM}(\hat{\mathbf{r}}) = \sum_{m,\sigma} (Lm, 1\sigma | JM)\, Y_{Lm}(\hat{\mathbf{r}})\; \mathbf{e}_\sigma, \tag{7}$$

where $(.., ..|..)$ are the Clebsch-Gordan coefficients and Y_{lm} are the normal spherical harmonics. The other widely used vector spherical harmonics are defined as

$$\mathbf{Y}^{(0)}_{JM}(\hat{\mathbf{r}}) \;=\; \mathbf{Y}^J_{JM}(\hat{\mathbf{r}}) \tag{8}$$

$$\mathbf{Y}^{(1)}_{JM}(\hat{\mathbf{r}}) \;=\; \sqrt{\frac{J+1}{2J+1}}\, \mathbf{Y}^{J-1}_{JM}(\hat{\mathbf{r}}) + \sqrt{\frac{J}{2J+1}}\, \mathbf{Y}^{J+1}_{JM}(\hat{\mathbf{r}}). \tag{9}$$

Following [44] we introduce a quantum number p defined as $p \equiv 1 - x$. It is $p = 0$ for electric multipoles and $p = 1$ for magnetic multipoles. The parity Π is $\Pi = (-1)^{L+p}$. This notation is different than in Devons and Goldfarb [40] and in Ferguson [41] where p defines the parity.

The coordinate system shown in Fig. 1 and the differential cross section expressed in Eq. 1 take the x axis along the photon propagation direction and z axis along the linear

polarization direction. This geometry is commonly adopted when the photons are highly linearly polarized as in the present experiment. However, a more general description of the photon polarization employs the Stokes parameters [45]. The Stokes parameters are defined in a reference frame in which the z axis is parallel to the photon momentum. The complete basis set to describe the photon polarization in this frame, due to the tranverse nature of the light, contains the left and right circular states, $|\mathbf{e}_{\lambda=+1}\rangle$ and $|\mathbf{e}_{\lambda=-1}\rangle$, respectively. So it is natural to transform the polarization part into that frame by

$$\rho_p = \sum_{\lambda,\lambda'} \sum_{\substack{L\,M\,p \\ L'M'p'}} \mathcal{D}^{L*}_{\lambda M}(\omega) \, \left| C^{1-p}_{L\lambda}(\hat{\mathbf{k}}_{\rm p}) \, \mathbf{a}^{1-p}_{LM}(\mathbf{r}) \right\rangle \left\langle C^{1-p'}_{L'\lambda'}(\hat{\mathbf{k}}_{\rm p}) \, \mathbf{a}^{1-p'}_{L'M'}(\mathbf{r}) \right| \, \mathcal{D}^{L'}_{\lambda' M'}(\omega), \tag{10}$$

with $\mathcal{D}$ as matrix elements of the Wigner rotation matrices and ω as Euler angles. Using the properties of the vector spherical harmonics [42] it can be shown that

$$\rho_p = \sum_{\Gamma\gamma} \sum_{\substack{L\,M\,x \\ L'M'x'}} (-)^{L-M} \, \widehat{\Gamma} \begin{pmatrix} L & L' & \Gamma \\ M & -M' & -\gamma \end{pmatrix} \mathcal{L}\,(p\,L, p'L')_{\Gamma\gamma} \, \left| \, \mathbf{a}^{1-p}_{LM}(\mathbf{r}) \, \right\rangle \left\langle \, \mathbf{a}^{1-p'}_{L'M'}(\mathbf{r}) \, \right| \tag{11}$$

with (in the Stokes parameter reference frame)

$$\begin{aligned} \mathcal{L}(p\,L, p'L')_{\Gamma\gamma_0} \;\equiv\; & 2\pi \, i^{L+p-L'-p'} \, \widehat{L}\,\widehat{L'} \sum_{\lambda\lambda'} \delta(\lambda, \pm 1)\delta(\lambda', \pm 1)(-\lambda)^p \, (-\lambda')^{p'} \\ & (-1)^{L-\lambda} \, \widehat{\Gamma} \begin{pmatrix} L & L' & \Gamma \\ \lambda & -\lambda' & -\gamma_0 \end{pmatrix} \rho^s_{\lambda\lambda'}, \end{aligned} \tag{12}$$

which transform to an arbitrary reference frame, like the one used in Eq. (11), like

$$\mathcal{L}(p\,L, p'L')_{\Gamma\gamma} = \sum_{\gamma_0} \mathcal{L}(p\,L, p'L')_{\Gamma\gamma_0} \mathcal{D}^{\Gamma*}_{\gamma_0\gamma}(\omega). \tag{13}$$

In Eqs. (11) and (12) Wigner 3J symbols have been used. The $\rho^s_{\lambda\lambda'}$ in Eq. (12) are the matrix elements of the polarization matrix ρ^s

$$\rho^s = \begin{pmatrix} \rho^s_{+1,+1} & \rho^s_{+1,-1} \\ \rho^s_{-1,+1} & \rho^s_{-1,-1} \end{pmatrix} = \frac{I}{2} \begin{pmatrix} 1+p_3 & -p_1+ip_2 \\ -p_1-ip_2 & 1-p_3 \end{pmatrix} \tag{14}$$

with the Stokes parameters I as total intensity and the polarization components p_1, p_2 and p_3 [45].

B. Molecular photoionization

First it is essential to derive a model to describe the aspects of the photoionization process we are interested in. The whole system can then be completely characterized by a density matrix. We have to specify the quantum states of the photons (see last section), the molecule, and the outgoing electron. We assume that the electrostatic interactions within the molecule are stronger than spin-orbit interactions and rotational interactions, i.e., we assume that Hund's coupling cases (a) and (b) apply (see for instance [46]). We denote the ground electronic state of the neutral molecule and the state of the singly charged molecular core by $|\Lambda_0\rangle$ and $|\Lambda_+\rangle$, respectively. In the following we will sum over unresolved vibrational states. We assume that the molecular orientation $\mathbf{m}$ does not change during the process. The outgoing electron will be in a well defined state $\left|\mathbf{k}_{\rm e}^{(-)}\right\rangle$ [47] with well defined spin $\mathbf{s}_{\rm e}$. The density matrix after photoionization by a single photon is therefore

$$\begin{aligned}\rho_a &= \left|\, \mathbf{m}\, \Lambda_+\, \mathbf{k}_{\rm e}^{(-)}\, \mathbf{s}_{\rm e}\, \right\rangle \left\langle\, \mathbf{m}\, \Lambda_+\, \mathbf{k}_{\rm e}^{(-)}\, \mathbf{s}_{\rm e}\, \right| \\ &= T \left|\, \mathbf{m}\, \Lambda_0\, \left(-\frac{a_{k_p}}{c}\right) \boldsymbol{\varepsilon}\, \exp\left(i\, \mathbf{k}_{\rm p}\cdot\mathbf{r}\right) \right\rangle \left\langle\, \mathbf{m}\, \Lambda_0\, \left(-\frac{a_{k_p}}{c}\right) \boldsymbol{\varepsilon}\, \exp\left(i\, \mathbf{k}_{\rm p}\cdot\mathbf{r}\right) \right| T^{+}, \end{aligned} \quad (15)$$

where T is the transition operator from the initial state to the final state. In this expression the state of a photon is not simply $|\boldsymbol{\varepsilon}\, \exp\left(i\, \mathbf{k}_{\rm p}\cdot\mathbf{r}\right)\rangle$ but rather $\left|-\left(a_{k_p}/c\right)\, \boldsymbol{\varepsilon}\, \exp\left(i\, \mathbf{k}_{\rm p}\cdot\mathbf{r}\right)\right\rangle$ with $a_{k_p} = c\sqrt{2\pi/\omega_p}$. The differential cross section is then [30]

$$\sigma(\mathbf{m}, \mathbf{k}_{\rm e}, \mathbf{s}_{\rm e}, \mathbf{k}_{\rm p}) = \frac{2\pi}{c}\, tr\left(\rho_a\right). \quad (16)$$

The last equations are general, but one has to be more specific to perform a calculation. The transition or interaction operator has several forms, depending on the approximation chosen ('length', 'velocity', 'acceleration') [29, 30, 48]. Ideally, the results of the calculation do not depend on the chosen form of the transition operator, but in practice each form is sensitive to particular regions of the molecular potential [29]. In the velocity form the non-relativistic transition operator for a certain photon multipole is

$$T^{v}_{LM_m}(p) = \mathbf{p}\cdot\mathbf{a}^{1-p}_{LM_m}(\mathbf{r}), \quad (17)$$

where $\mathbf{p} = -i\,\boldsymbol{\nabla}$ is the momentum operator of the electron. The operator in Eq. 17 is defined in the molecular body frame. (Throughout the article quantum numbers in that frame are denoted by an index m.) It is useful intuitively to calculate the transition amplitudes in

this frame due to the decreased symmetry of molecular potentials compared to atoms. To derive the length form of the transition operator we use [48, 49]

$$\mathbf{p} = i\ [H, \mathbf{r}]\,. \tag{18}$$

If ψ and ψ' are eigenfunctions of H with eigenvalues E and E', respectively, the electronic transition amplitudes in length and velocity forms are related by

$$\langle\psi'|\,\mathbf{p}\cdot\mathbf{a}^1_{1M_m}(\mathbf{r})\,|\psi\rangle \;=\; i\,\omega\,\langle\psi'|\,\mathbf{r}\cdot\mathbf{a}^1_{1M_m}(\mathbf{r})\,|\psi\rangle\,, \tag{19}$$

$$\langle\psi'|\,\mathbf{p}\cdot\mathbf{a}^1_{2M_m}(\mathbf{r})\,|\psi\rangle \;=\; i\,\frac{\omega}{2}\,\langle\psi|\,\mathbf{r}\cdot\mathbf{a}^1_{2M_m}(\mathbf{r})\,|\psi'\rangle\,, \tag{20}$$

with $\omega = E' - E$. Here $\omega = \omega_p$, since the energy of the system is changed by absorption of one photon. Since Eqs. 19 and 20 are based on the assumption that ψ and ψ' are eigenfunctions of H, they are sensitive to the quality of the wavefunctions used in calculations. The nature of the magnetic interaction is different from the electric one, because in first order the angular momentum does not change. In the magnetic dipole operator this is reflected by the cross product $\mathbf{L} = \mathbf{r} \times \mathbf{p}$. The components of the operator are

$$T_{LM_m}(1) = i\,k_p\,\frac{1}{\sqrt{24\pi}} L_{M_m}. \tag{21}$$

The magnetic dipole transition operator exists only in one form. The transition operators seem to be different from their dyadic forms [48, 49]. This is due to the detachment of the polarization in our notation. If the polarization is included the operators again become identical to their dyadic forms

$$\mathbf{p}\cdot\sum_M C^1_{1M}(\hat{\mathbf{k}}_\mathrm{p})\,\mathbf{a}^1_{1M}(\mathbf{r}) \;=\; \mathbf{p}\cdot\boldsymbol{\varepsilon}, \tag{22}$$

$$\mathbf{p}\cdot\sum_M C^0_{1M}(\hat{\mathbf{k}}_\mathrm{p})\,\mathbf{a}^0_{1M}(\mathbf{r}) \;=\; \frac{i}{2}\left((\mathbf{k}_\mathrm{p}\times\boldsymbol{\varepsilon})\,(\mathbf{r}\times\mathbf{p})\right), \tag{23}$$

$$\mathbf{p}\cdot\sum_M C^1_{2M}(\hat{\mathbf{k}}_\mathrm{p})\,\mathbf{a}^1_{2M}(\mathbf{r}) \;=\; \frac{i}{2}\left((\boldsymbol{\varepsilon}\cdot\mathbf{p})\,(\mathbf{k}_\mathrm{p}\cdot\mathbf{r}) + (\boldsymbol{\varepsilon}\cdot\mathbf{r})\,(\mathbf{k}_\mathrm{p}\cdot\mathbf{p})\right). \tag{24}$$

In the following we will chose an ansatz in which partial waves are employed. The electronic wavefunction $\left|\mathbf{k}_\mathrm{e}^{(-)}\right\rangle$ is expanded into spherical harmonics [50]. However, due to the non-spherical molecular potential, only the projection of the angular momentum on the molecular axis is a good quantum number – not the angular momentum itself. Dipole selection rules therefore do not restrict the expansion of $\left|\mathbf{k}_\mathrm{e}^{(-)}\right\rangle$, as they do in atoms. Nevertheless, convergence of the partial wave expansion is reached quite rapidly. To a very good approximation, a limited number of terms is sufficient, and the expansion can be truncated at a certain l_{max}.

In the following we assume that the spin of the electron will not be detected. (On how to incorporate the spin as well and for more details in general, see [51]). Integration over the electronic spin leads to

$$\left\langle \mathbf{m}\,\Lambda_+\,\mathbf{k}_{\rm e}^{(-)}\,\middle|\,\rho\,\middle|\,\mathbf{m}\,\Lambda_+\,\mathbf{k}_{\rm e}^{(-)}\right\rangle \equiv \frac{\sqrt{2}}{4\,\pi}\int \left\langle \mathbf{m}\,\Lambda_+\,\mathbf{k}_{\rm e}^{(-)}\,\mathbf{s}_{\rm e}\,\middle|\,\rho_a\,\middle|\,\mathbf{m}\,\Lambda_+\,\mathbf{k}_{\rm e}^{(-)}\,\mathbf{s}_{\rm e}\right\rangle\,d\mathbf{s}_{\rm e}. \tag{25}$$

After some extensive Racah algebra and considering Eq. 16, one gets for the cross section

$$\sigma(\mathbf{m},\mathbf{k}_{\rm e},\mathbf{k}_{\rm p}) = \frac{4\pi^2}{\omega_p\,c}\sum_{pp'}\sum_{LL'}\sum_{d\mathcal{L}\Gamma} M_{d\mathcal{L}\Gamma}(p\,L,p'L')\,F_{d\mathcal{L}\Gamma}(p\,L,p'L'). \tag{26}$$

Two types of terms are introduced in Eq. 26, i.e., dynamical or kinematical terms, $M(p\,L,p'L')_{d\mathcal{L}\Gamma}$, and geometrical terms, $F(p\,L,p'L')_{d\mathcal{L}\Gamma}$, which contain all dependencies on the dynamics and geometries, respectively, of the molecular single photoionization process. In particular they are defined as

$$F_{d\mathcal{L}\Gamma}(p\,L,p'L') = \sum_{\gamma}\mathcal{L}(p\,L,p'L')_{\Gamma\gamma}\,Y^{d\mathcal{L}}_{\Gamma\gamma}(\mathbf{m},\hat{\mathbf{k}}_{\rm e}), \tag{27}$$

where $Y^{d\mathcal{L}}_{\Gamma\gamma}$ are the bipolar spherical harmonics [42]; and as

$$\begin{aligned} M_{d\mathcal{L}\Gamma}(p\,L,p'L') = {} & \widehat{d}\,\widehat{\mathcal{L}}\sum_{M_m M'_m}\sum_{\substack{lm_m\\ l'm'_m}}(-)^{L+M_m+m'_m+\Gamma}\,\widehat{l}\,\widehat{l'} \\ & \begin{pmatrix} l & l' & \mathcal{L}\\ 0 & 0 & 0\end{pmatrix}\begin{pmatrix} l & l' & \mathcal{L}\\ -m_m & m'_m & -\alpha_m\end{pmatrix}\begin{pmatrix} L & L' & \Gamma\\ M_m & -M'_m & \alpha_m\end{pmatrix}\begin{pmatrix} d & \mathcal{L} & \Gamma\\ 0 & \alpha_m & -\alpha_m\end{pmatrix} \\ & i^{l-l'}\,\exp\left(i(\Delta_l-\Delta_{l'})\right)\left\langle\Lambda_+\,lm_m\right|T_{LM_m}(p)\left|\Lambda_0\right\rangle\left\langle\Lambda_+\,l'm'_m\right|T_{L'M'_m}(p')\left|\Lambda_0\right\rangle^*. \end{aligned} \tag{28}$$

Here $\left\langle\Lambda_+\,lm_m\right|T_{LM_m}(p)\left|\Lambda_0\right\rangle$ are the complex transition amplitudes.

It is evident that a large number of dynamical coefficients must be calculated to derive the angular distribution of photoelectrons from fixed-in-space molecules. However, one can deduce some useful dependencies and decrease the number of non-redundant coefficients dramatically. From Eq. 28 follows

$$M_{d\mathcal{L}\Gamma}(p\,L,p'L') = (-)^{L+L'+d+\mathcal{L}+\Gamma}\,M_{d\mathcal{L}\Gamma}(p'L',p\,L)^*. \tag{29}$$

Furthermore, parity conservation restricts the values of $\mathcal{L}$: $\mathcal{L}$ and the sum $(p+L+p'+L')$ are both either even or odd. Additional restrictions arise from symmetries of the molecular potential [52]: (a) if a molecule possesses a center of symmetry then there exists a basis of

energy eigenfunctions with defined symmetry. (Obviously, heteronuclear molecules do not have such a symmetry center.) Now if the initial and final molecular states have a well defined parity, then due to parity conservation $\mathcal{L}$ just has even values and (b) the matrix elements for molecules with cylindrical symmetry are invariant if the signs of all projection quantum numbers on the cylinder axis are changed.

Considering these restrictions one gets for the angle-integrated cross section σ

$$\sigma = \int\int\int \sigma(\mathbf{m}, \mathbf{k}_\mathrm{e}, \mathbf{k}_\mathrm{p})\, d\mathbf{m}\, d\mathbf{k}_\mathrm{e}\, d\mathbf{k}_\mathrm{p} \tag{30}$$

$$= \frac{4\pi^2}{\omega_p\, c}\, 4\,\pi \sum_{\{pL\}} \frac{\widehat{L}}{2}\, M_{000}(pL, pL). \tag{31}$$

The cross section in dipole approximation is therefore

$$\sigma = \frac{4\pi^2}{\omega_p\, c}\, 4\,\pi \frac{\sqrt{3}}{2}\, M_{000}(01, 01). \tag{32}$$

With the equations derived so far a detailed analysis of photoionization processes beyond the dipole approximation is possible. Many possibilities arise. However, in the following we will focus on ongoing experiments. If one considers multipole terms up to first order only, i.e. $E1$, $M1$, $E2$ terms, then the differential cross section is given by Eq. 1, and the angular distribution parameters are expressed

$$\beta_e = -\sqrt{10}\, M_{022}(01, 01)/M_{000}(01, 01) \tag{33}$$

$$\delta = \left[3\sqrt{2}\,(M_{011}(01, 11) - M_{011}(01, 02)) - 2\sqrt{7} M_{033}(01, 02)\right]/M_{000}(01, 01) \tag{34}$$

$$\gamma = 10\sqrt{7} M_{033}(01, 02)/M_{000}(01, 01). \tag{35}$$

In the last equations only electric dipole contributions and interference terms of electric dipole and magnetic dipole/electric quadrupole are considered. Those should still be much larger than terms of higher order than dipole alone. We also obtain an expression for the molecular alignment anisotropy parameter β_m [14] by averaging the dipole photoelectron angular distribution over the electronic orientation:

$$\beta_m = -\sqrt{10}\, M_{202}(01, 01)/M_{000}(01, 01). \tag{36}$$

For the calculations, we used codes developed at the California Institute of Technology (for an early reference see [38]). As a check for the quality of the wave functions used, the transition amplitudes in both length and velocity form were calculated. The velocity form results are compared with measurements in Section IV.

III. EXPERIMENTAL METHODS

The experiments were done at the University of Wisconsin's Synchrotron Radiation Center using a tunable, linearly polarized photon beam provided by an undulator and plane grating monochromator [53]. The bandwidth varied from 0.005 eV to 0.130 eV over the 20–150 eV photon energy range. The flux over that energy range was $\sim 10^9 - 10^{10}$ photons/(s·mA), and the stored electron current varied over 100–200 mA. The undulator was stepped along with the monochromator at each energy to maintain maximum flux and a degree of linear polarization >0.99 [54]. Photoelectron intensities were normalized to the photocurrents from nickel meshes located at the front and back of the spectrometer chamber.

The electron spectrometer system and measurement methods have been described in Refs. [23, 27]. As shown in Fig. 1, the coordinate system is defined by the propagation vector $\mathbf{k}$ along x and photon beam polarization vector $\boldsymbol{\epsilon}$ along z. Four 45°-parallel-plate electron analyzers (PPAs) [55] are mounted on a rotation stage with its rotation axis along the y axis, i.e., perpendicular to both $\mathbf{k}$ and $\boldsymbol{\epsilon}$. The angular positions of the PPAs are fixed at 125.3° with respect to the rotation axis. At the positions shown in Fig. 1 and the top frame of Fig. 2, the PPAs accept photoelectrons emitted at angles that are "magic" with respect to all three coordinate axes, i.e., the direction cosines are all $\pm 1/\sqrt{3}$. At these angles, $P_2(\cos\theta) = 0$, and the dependence on β_e vanishes in Eq. 1. Defining N_1, N_2, N_3, and N_4 to be the photoelectron intensities at these "nondipole" angles, the combined asymmetry parameter is given by

$$\gamma + 3\delta = \sqrt{27}\left(\frac{N_1 - N_2 - N_3 + N_4}{N_1 + N_2 + N_3 + N_4}\right). \tag{37}$$

Note that the sum of the photoelectron intensities, $N_1 + N_2 + N_3 + N_4$, is independent of β_e, γ, and δ and is proportional to the angle-integrated cross section σ. Equation 37 shows that $\gamma + 3\delta$ is given by the forward–backward asymmetry of photoelectron intensities with respect to $\mathbf{k}$ normalized to the angle-integrated intensity.

Rotating the analyzers by 45° about y places them as shown in the bottom frame of Fig. 2. At that position, the polar angles of PPAs 1 and 3 are $\theta = 90° \pm 54.7°$, where 54.7° is a magic angle, and the polar angles of PPAs 2 and 4 are $\theta = 90°$. $P_2(\cos\theta)$ is nonzero at those angles, and the photoelectron intensities depend on β_e. Defining D_1, D_2, D_3, and D_4 to be the photoelectron intensities at these "dipole" angles, the β_e parameter is given by

either of the following two equations:

$$\beta_e = 4\left(\frac{s_0}{s_\perp}\right)\left(\frac{D_1 + D_3}{N_1 + N_2 + N_3 + N_4}\right) - 2 \tag{38}$$

and

$$\beta_e = 2 - 4\left(\frac{s_0}{s_\parallel}\right)\left(\frac{D_2 + D_4}{N_1 + N_2 + N_3 + N_4}\right). \tag{39}$$

The parameters s_0, $s_\perp$, and $s_\parallel$ in Eqs. 38 and 39 represent the different fractions of the photoelectron source volume observed by the PPAs at different angular positions. The source volume has a cylindrical shape produced by the photon beam passing through the gas jet. s_0 represents the fraction of the source volume observed by the PPAs at the nondipole angles depicted in the top frame of Fig. 2. All PPAs observe the same fraction, so s_0 does not appear in Eq. 37. At the dipole angles shown in the bottom frame of Fig. 2, PPAs 1 and 3 are perpendicular to the photon beam and observe a source volume fraction $s_\perp$, while PPAs 2 and 4 are parallel to the photon beam and observe a source volume fraction $s_\parallel$. The ratios $s_0/s_\perp$ and $s_0/s_\parallel$ can be determined by inverting Eqs. 38 and 39 and measuring photoelectron intensities from transitions of known β_e values. The He 1s $\beta_e = 2$ at photon energies below the doubly-excited states near ∼60 eV, and the Ne 2p β_e vs. energy is accurately known through measurements and theory [56–61]. Measurements of He 1s and Ne 2p photoelectrons were used to determine $s_0/s_\perp = 1.1 - 1.2$ over the 5–130 eV kinetic energy range. β_e values for H_2 were then determined using Eq. 38. Equation 39 was not used, because He and H_2 both have large β_e values for which the D_2 and D_4 intensities are weak. For each photon energy, the rotation platform was positioned at eight angles in steps of 45° so that each PPA recorded photoelectron intensities at the eight positions indicated in Fig. 2, and the results from the four analyzers were averaged.

Photoelectron spectra of H_2 have been recorded that resolve vibrational and rotational structure of the H_2^+ ion [8, 9]. The goal of the present experiments was to accurately measure vibrationally averaged angular distributions for comparison with fixed-nuclei calculations. The PPAs were operated at fixed pass energies of 100 eV, and the kinetic energy resolution was measured to be 2.2 eV full width at half maximum (FWHM). A constant ionic state (CIS) method was used to record photoelectron intensities vs. photon energy [27]. In this technique, the potentials on the PPAs are stepped along with the photon energy and undulator energy to record photoelectron intensities at fixed ionization energy of the atom or molecule. Accounting for the 2.2 eV FWHM kinetic energy resolution, the ionization energy

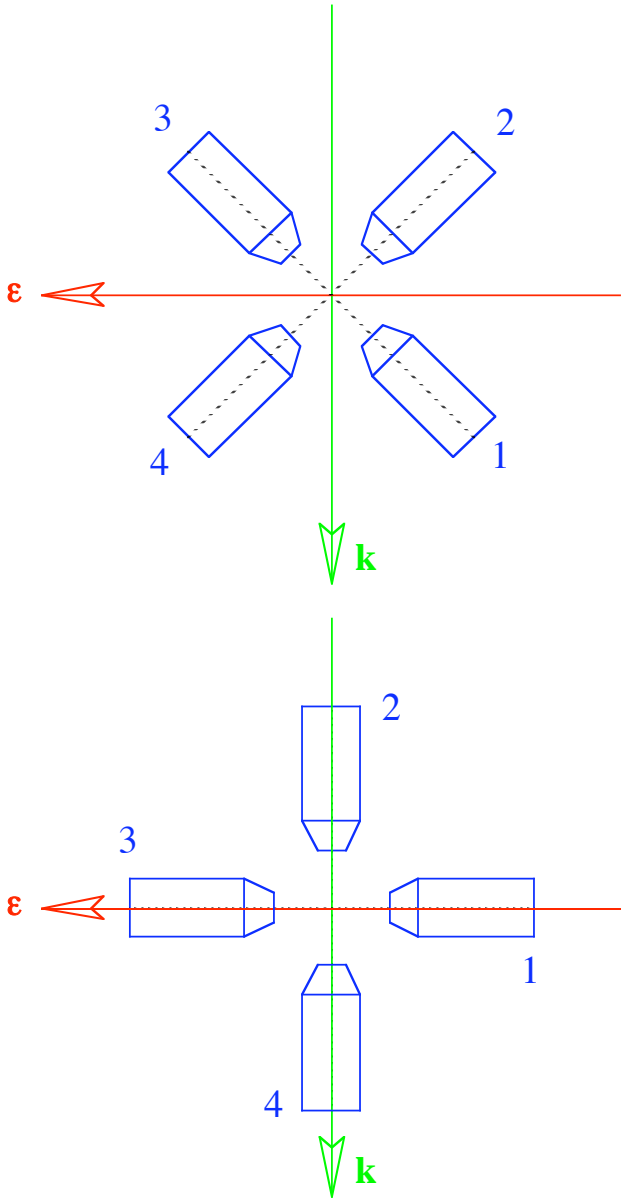

Figure 2: (Color online) The positions of the four electron analyzers projected onto the $\boldsymbol{\epsilon}$-$\mathbf{k}$ plane. The top frame shows the positions used to measure nondipole asymmetries $\gamma + 3\delta$. The bottom frame shows the positions used to measure dipole anisotropies β_e.

band measured for H_2 was 16.4 ± 1.1 eV. Comparison with the high resolution spectrum [8] shows that the peak of the ionization energy band was near the $v' = 4$ vibrational level of H_2^+ and the band encompassed $v' = 0 - 10$.

Contact potentials and stray electric and magnetic fields should be minimized for accurate measurements of photoelectron angular distributions, particularly for low kinetic energies.

Technical improvements were made since our previous experiments [23, 27, 31, 37] to further reduce spurious effects. The vacuum chamber is shielded with two layers of high permeability mu-metal that reduce the magnetic field to <1 mG. However, stray magnetic fields can be produced by steel spectrometer parts, so those were replaced with parts made of nonmagnetic materials. With the PPAs mounted on the rotation platform, the magnetic field in the interaction region varied within 0.35–0.75 mG as the platform was rotated by 360°. The gas nozzle was made of copper capillary tubing and was positioned ∼1 mm above the photon beam. The gas nozzle and PPA entrance snouts were coated with colloidal graphite to reduce contact potentials.

Photoelectrons of kinetic energy E_k are emitted from the interaction region, enter a PPA snout, and pass through a grid that accelerates or decelerates them to the pass energy E_p (100 eV for these experiments). The potential on this grid is the same as the potential V_l on the lower plate of the PPA. According to the electron-optical model of a 45° PPA [55], the upper plate should be at the potential $V_u = V_l + 0.6E_p$, where 0.6 is referred to as the "spectrometer factor". By stepping the potentials V_l and V_u according to this relation, the photoelectron spectrum can be recorded at a given photon energy, or a CIS scan can be recorded by stepping the potentials along with the photon energy. However, the measured spectrometer factors are slightly different from 0.6 for each PPA. Consequently, since V_l and V_u for the four PPAs are provided by the same two voltage sources, the measured photoelectron spectra do not accurately match or track with changes in photon energy. Five equally-spaced field-termination plates are mounted between the upper and lower plates of each PPA, and an internal voltage divider determines the potentials on the seven plates. To match the spectrometer factors of the four PPAs, external trim resistors were added between the V_u source and the voltage divider. To account for individual contact potentials, externally adjustable offsets were added to V_l for each PPA. Also, the gas nozzle was electrically isolated and biased to -0.15 V to account for its contact potential. These procedures resulted in photoelectron spectra well matched to known ionization energies of the rare gases and H_2. The CIS method was tested at selected photon energies by scanning the entire He 1s, Ne 2p, or H_2 photoelectron spectra at the eight positions of the rotation platform as described earlier. Relative photoelectron intensities at the peak maxima agree well with intensities summed over the entire spectra for each PPA at the eight angular positions. With these technical improvements, the β_e and $\gamma + 3\delta$ parameters could be measured to as low as ∼3

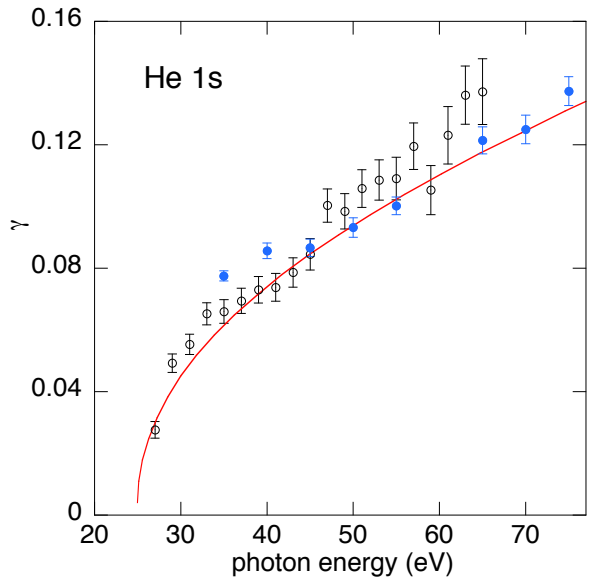

Figure 3: (Color online) Nondipole asymmetry parameter γ of He 1s photoelectrons. The present results (open circles) are compared with previous measurements (closed circles) and RPAE calculations from Ref. [27].

eV kinetic energy.

IV. RESULTS AND DISCUSSION

As discussed above, He 1s and Ne 2p photoelectrons were used to determine relative source volumes observed by the electron analyzers in measurements of β_e parameters. The nondipole asymmetries derived from those measurements are plotted in Figs. 3 and 4. The He 1s measurements agree well with earlier measurements and with calculated asymmetries using the random phase approximation with exchange (RPAE) [27]. The present measurements confirm the RPAE calculations at lower kinetic energies. For Ne 2p, the RPAE calculations of Ref. [26] match the measured asymmetries fairly well, although with small deviations at lower kinetic energies.

Our primary results are shown in Fig. 5 where the calculated photoionization parameters of H_2 are compared with measurements over the 20–180 eV photon energy range. The calculated total cross section σ in panel 5(a) is in excellent agreement with measurements [4]. The present measurements of β_e and $\gamma+3\delta$ are compared with the calculated curves in panels

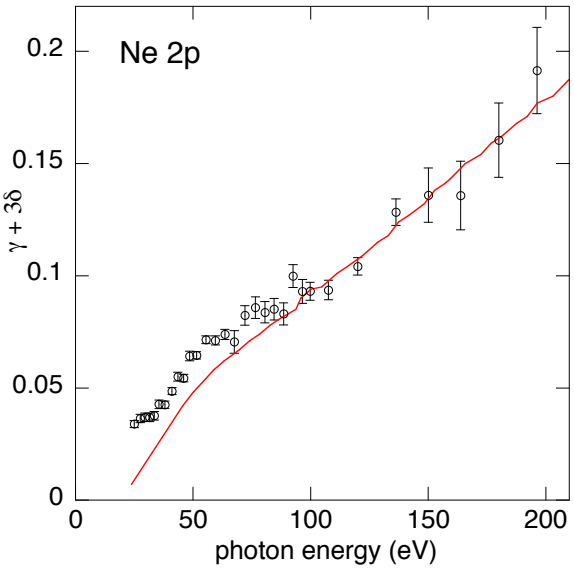

Figure 4: (Color online) Nondipole asymmetry parameter $\gamma + 3\delta$ of Ne 2p photoelectrons. The present measurements (open circles) are compared with RPAE calculations from Ref. [26].

5(b) and 5(c). Good overall agreement is observed for the magnitudes and energy variations of these parameters. The measured β_e passes through a minimum near 30 eV. Doubly-excited states appear in this energy region [10–12], and oscillations in the β_e parameter are predicted when doubly-excited states are included in calculations [12]. The observed feature does not appear in the present calculations that do not treat doubly-excited states. The deviation of the measured $\gamma + 3\delta$ parameter from the calculated curve in the 20–30 eV range may also be due to the doubly-excited states. The measured β_e and $\gamma + 3\delta$ parameters also deviate from the calculated curves at energies above 100 eV. Our calculations employ partial wave expansions which might not be fully converged at higher energies. This could account for some of the difference between measurements and calculations. At lower energies our method provides converged solutions for the photoelectron within the limitations of the assumed static-exchange potential.

The molecular alignment anisotropy parameter β_m is sensitive to the relative strengths of the $\Sigma \rightarrow \Sigma$ and $\Sigma \rightarrow \Pi$ dipole transitions, and can be determined from measurements of the angular distributions of protons ejected in dissociative photoionization [14]. Kossmann *et al.* [6] determined β_m parameters for double photoionization of H_2 over 52–110 eV, and their measurements are compared with the calculated curve in Fig. 5(d). Although the

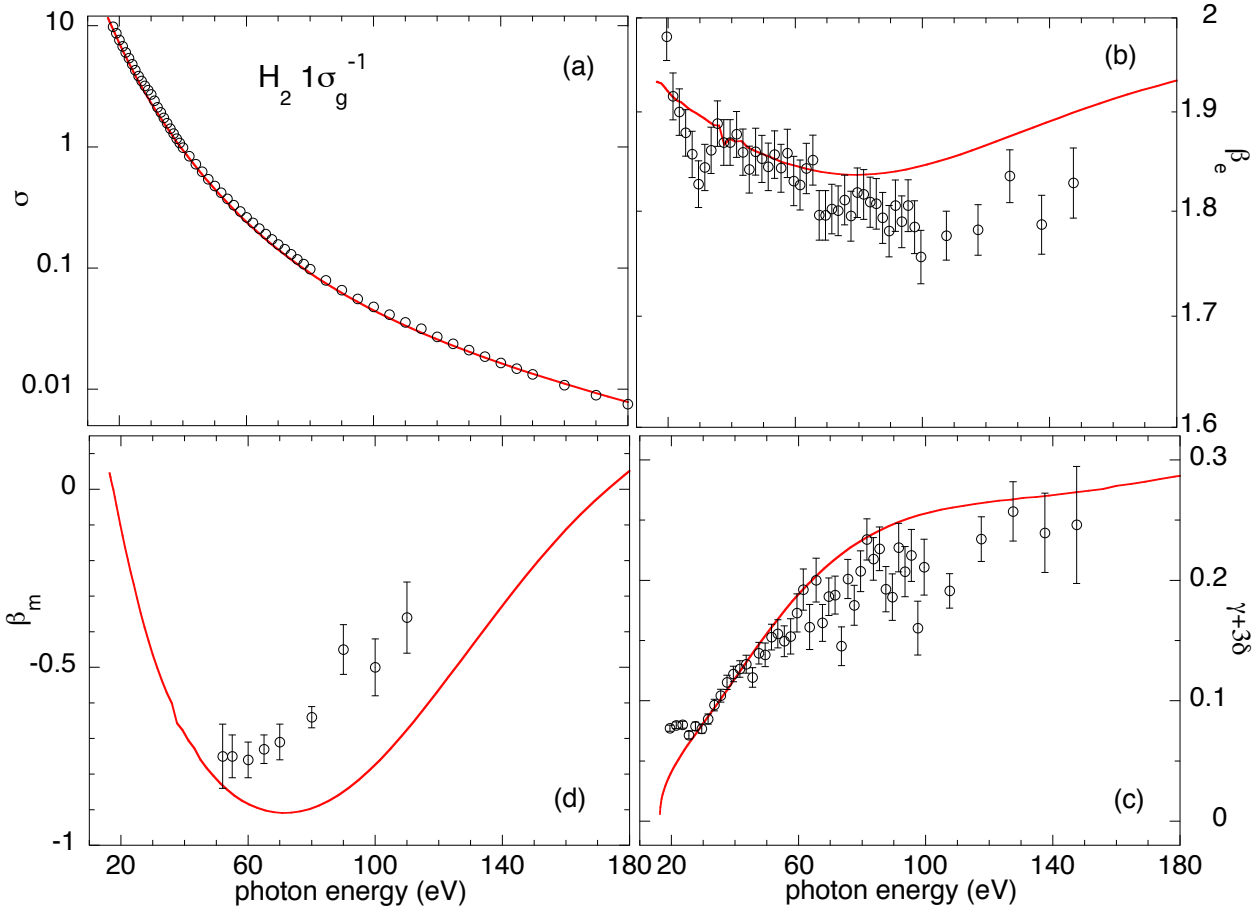

Figure 5: (Color online) Calculated and measured photoionization parameters of molecular H_2. (a) Total cross section σ compared with measurements from Ref. [4]. (b) Electric dipole anisotropy parameter β_e compared with present measurements. (c) Nondipole asymmetry parameter $\gamma + 3\delta$ compared with present measurements. (d) Molecular alignment anisotropy parameter β_m compared with double photoionization measurements from Ref. [6].

calculations are not for the double photoionization process, the calculated β_m shows a similar magnitude and energy variation as the measurements. The β_m parameter is negative due to the strength of the $\Sigma \rightarrow \Pi$ transition [14] and passes through a broad minimum as the relative strengths of the two dipole symmetries vary with energy.

V. CONCLUSION

We present a theory of molecular photoionization that includes cross terms of electric dipole ($E1$) amplitudes with electric quadrupole ($E2$) and magnetic dipole ($M1$) amplitudes that give rise to nondipole asymmetries in photoelectron angular distributions. The photoionization cross section, dipole and nondipole photoelectron angular distribution parameters, and the molecular alignment parameter of H_2 are calculated over 20–180 eV and compared with measurements. We describe new measurements of the dipole and nondipole photoelectron angular distribution parameters. The calculations are in excellent agreement with measured total cross sections [4] and compare well overall with the magnitudes and energy variations of the photoelectron angular distribution parameters. The measured parameters show features attributed to doubly-excited states [12].

The theory, calculations, and measurements presented here for H_2 and for N_2 in Ref. [37] show that nondipole asymmetries provide insight into low energy photoionization that adds to the numerous observations that can be treated within the dipole approximation. Future work could include other diatomic and polyatomic molecules, vibrationally resolved results, and studies of double excitation and other interchannel interactions. In related work, there is significant interest in confinement resonances that arise in photoionization of atoms contained in C_{60} molecular cages [62]. Strong nondipole effects have been predicted in photoionization calculations on confined atoms [63, 64].

VI. ACKNOWLEDGEMENTS

We thank the staff of the Synchrotron Radiation Center for technical support. The SRC was previously supported by the National Science Foundation and the University of Wisconsin–Madison. BZ thanks the Alexander von Humboldt Foundation for a Feodor Lynen fellowship. SHS, EPK, and BK were supported by the U.S. Department of Energy, Office of Science, Chemical Sciences, Geosciences, and Biosciences Division under contract no. DE-AC02-06CH11357.

---

[1] A. Dalgarno, J. Chem. Soc. Faraday Trans. **89**, 2111 (1993).

[2] M. Yan, H. R. Sadeghpour, and A. Dalgarno, Astrophys. J. **496**, 1044 (1998).

[3] Y. M. Chung, E.-M. Lee, T. Masuoka, and J. A. R. Samson, J. Chem. Phys. **99**, 885 (1993).

[4] J. A. R. Samson and G. N. Haddad, J. Opt. Soc. Am. B **11**, 277 (1994).

[5] W. A. Chupka, P. M. Dehmer, and W. T. Jivery, J. Chem. Phys. **63**, 3929 (1975).

[6] H. Kossmann, O. Schwarzkopf, B. Kämmerling, and V. Schmidt, Phys. Rev. Lett. **63**, 2040 (1989).

[7] J. L. Dehmer, P. M. Dehmer, J. B. West, M. A. Hayes, M. R. F. Siggel, and A. C. Parr, J. Chem. Phys. **97**, 7911 (1992).

[8] J. E. Pollard, D. J. Trevor, J. E. Ruett, Y. T. Lee, and D. A. Shirley, J. Chem. Phys. **77**, 34 (1982).

[9] G. Öhrwall, P. Baltzer, and J. Bozek, J. Phys. B **32**, L51 (1999).

[10] Z. X. He, J. N. Cutler, S. H. Southworth, L. R. Hughey, and J. A. R. Samson, J. Chem. Phys. **103**, 3912 (1995).

[11] I. Sánchez and F. Martín, J. Chem. Phys. **107**, 8391 (1997).

[12] I. Sánchez and F. Martín, J. Phys. B **30**, 679 (1997).

[13] A. C. Parr, J. E. Hardis, S. H. Southworth, C. S. Feigerle, F. M. Quinn, B. R. Dobson, J. B. West, G. V. Marr, and J. L. Dehmer, Phys. Rev. A **37**, 437 (1988).

[14] J. L. Dehmer and D. Dill, Phys. Rev. A **18**, 164 (1978).

[15] J. D. Bozek, J. E. Furst, T. J. Gay, H. Gould, A. L. D. Kilcoyne, J. R. Machacek, F. Martín, K. W. McLaughlin, and J. L. Sanz-Vicario, J. Phys. B **39**, 4871 (2006).

[16] J. L. Sanz-Vicario, H. Bachau, and F. Martín, Phys. Rev. A **73**, 033410 (2006).

[17] A. Staudte, D. Pavičić, S. Chelkowski, D. Zeidler, M. Meckel, H. Niikura, M. Schöffler, S. Schössler, B. Ulrich, P. P. Rajeev, et al., Phys. Rev. Lett. **98**, 073003 (2007).

[18] F. Martín, J. Fernández, T. Havermeier, L. Foucar, Th. Weber, K. Kreidi, M. Schöffler, L. Schmidt, T. Jahnke, O. Jagutzki, et al., Science **315**, 629 (2007).

[19] J. Fischer, Ann. Phys. (Leipzig) **8**, 821 (1931).

[20] A. Sommerfeld, *Wave Mechanics* (Methuen & Co., London, 1930), 2nd ed.

[21] A. Bechler and R. H. Pratt, Phys. Rev. A **39**, 1774 (1989).

[22] A. Bechler and R. H. Pratt, Phys. Rev. A **42**, 6400 (1990).

[23] B. Krässig, J.-C. Bilheux, R. W. Dunford, D. S. Gemmell, S. Hasegawa, E. P. Kanter, S. H. Southworth, L. Young, L. A. LaJohn, and R. H. Pratt, Phys. Rev. A **67**, 022707 (2003).

[24] J. W. Cooper, Phys. Rev. A **47**, 1841 (1993).

[25] W. R. Johnson and K. T. Cheng, Phys. Rev. A **63**, 022504 (2001).

[26] M. Ya. Amusia, A. S. Baltenkov, L. V. Chernysheva, Z. Felfli, and A. Z. Msezane, Phys. Rev. A **63**, 052506 (2001).

[27] E. P. Kanter, B. Krässig, S. H. Southworth, R. Guillemin, O. Hemmers, D. W. Lindle, R. Wehlitz, M. Y. Amusia, L. V. Chernysheva, and N. L. S. Martin, Phys. Rev. A **68**, 012714 (2003).

[28] S. H. Southworth, R. W. Dunford, E. P. Kanter, B. Krässig, L. Young, L. A. LaJohn, and R. H. Pratt, Radiat. Phys. Chem. **75**, 1574 (2006).

[29] A. F. Starace, in *Handbuch der Physik*, edited by W. Mehlhorn (Springer-Verlag, Berlin, 1982), vol. 31, pp. 1–121.

[30] M. Ya. Amusia, *Atomic Photoeffect* (Plenum Press, New York, 1990).

[31] O. Hemmers, R. Guillemin, E. P. Kanter, B. Krässig, D. W. Lindle, S. H. Southworth, R. Wehlitz, J. Baker, A. Hudson, M. Lotrakul, et al., Phys. Rev. Lett. **91**, 053002 (2003).

[32] B. Krässig, E. P. Kanter, S. H. Southworth, L. Young, R. Wehlitz, B. A. deHarak, and N. L. S. Martin, Phys. Rev. A **86**, 053408 (2012).

[33] P. W. Langhoff, J. C. Arce, J. A. Sheehy, O. Hemmers, H. Wang, P. Focke, I. A. Sellin, C. Heske, and D. W. Lindle, J. Electron Spectrosc. Relat. Phenom. **114-116**, 23 (2001).

[34] A. N. Grum-Grzhimailo, J. Phys. B **36**, 2385 (2003).

[35] K. Hosaka, J. Adachi, A. V. Golovin, M. Takahashi, T. Teramoto, N. Watanabe, A. Yagishita, S. K. Semonov, and N. A. Cherepkov, J. Phys. B **39**, L25 (2006).

[36] D. Toffoli and P. Decleva, J. Phys. B **39**, 2681 (2006).

[37] O. Hemmers, R. Guillemin, D. Rolles, A. Wolska, D. W. Lindle, E. P. Kanter, B. Krässig, S. H. Southworth, R. Wehlitz, B. Zimmermann, et al., Phys. Rev. Lett. **97**, 103006 (2006).

[38] R. R. Lucchese, G. Raseev, and V. McKoy, Phys. Rev. A **25**, 2572 (1982).

[39] M. E. Rose, *Multipole Fields* (John Wiley & Sons, New York, 1955).

[40] S. Devons and L. J. B. Goldfarb, in *Handbuch der Physik*, edited by Springer-Verlag (Springer-Verlag, Berlin, 1957), vol. 42, p. 392.

[41] A. J. Ferguson, *Angular Correlation Methods in Gamma-Ray Spectroscopy* (John Wiley & Sons, New York, 1965).

[42] D. A. Varshalovich, A. N. Moskalev, and A. K. Khersonskii, *Quantum Theory of Angular*

Momentum (World Scientific, Singapore, 1988), p. 228.

[43] W. R. Johnson and F. D. Feiock, Phys. Rev. **168**, 22 (1968).

[44] V. V. Balashov, A. N. Grum-Grzhimailo, and N. M. Kabachnik, *Polarization and Correlation Phenomena in Atomic Collisions - A Practical Theory Course* (Kluwer Academic/Plenum, New York, 2000).

[45] K. Blum, *Density Matrix Theory and Applications* (Plenum Press, New York, 1981).

[46] E. E. Nikitin and R. N. Zare, Mol. Phys. **82**, 85 (1994).

[47] L. D. Landau and E. M. Lifshitz, *Course of Theoretical Physics, Vol. 3: Quantum Mechanics: Non-Relativistic Theory* (Pergamon, New York, 1977), 3rd ed.

[48] H. A. Bethe and E. E. Salpeter, *Quantum Mechanics of One- and Two-Electron Atoms* (Springer-Verlag, Berlin, 1958).

[49] J. R. Haskins, Am. J. Phys. **46**, 402 (1978).

[50] D. Dill, J. Chem. Phys. **65**, 1130 (1976).

[51] B. Zimmermann, in *Studies of Vacuum Ultraviolet and X-ray Processes*, edited by U. Becker (Wissenschaft und Technik Verlag, Berlin, 2000), vol. 13.

[52] N. A. Cherepkov and V. V. Kuznetsov, Z. Phys. D **7**, 271 (1987).

[53] R. Reininger, S. L. Crossley, M. A. Lagergren, M. C. Severson, and R. W. C. Hansen, Nucl. Instrum. Methods A **347**, 304 (1994).

[54] S. B. Whitfield, K. Caspary, T. Myers, M. Bjelland, R. Wehlitz, J. Jiménez-Mier, P. Olalde-Velasco, and M. O. Krause, J. Phys. B **38**, 3273 (2005).

[55] G. A. Harrower, Rev. Sci. Instrum. **26**, 850 (1955).

[56] F. Wuilleumier and M. O. Krause, Phys. Rev. A **10**, 242 (1974).

[57] J. L. Dehmer, W. A. Chupka, J. Berkowitz, and W. T. Jivery, Phys. Rev. A **12**, 1966 (1975).

[58] W. R. Johnson and K. T. Cheng, Phys. Rev. A **20**, 978 (1979).

[59] H. Derenbach, R. Malutzki, and V. Schmidt, Nucl. Instrum. Methods **208**, 845 (1983).

[60] S. H. Southworth, A. C. Parr, J. E. Hardis, J. L. Dehmer, and D. M. P. Holland, Nucl. Instrum. Methods A **246**, 782 (1986).

[61] O. Hemmers, M. Blackburn, T. Goddard, P. Glans, H. Wang, S. B. Whitfield, R. Wehlitz, I. A. Sellin, and D. W. Lindle, J. Electron Spectrosc. Relat. Phenom. **123**, 257 (2002).

[62] R. A. Phaneuf, A. L. D. Kilcoyne, N. B. Aryal, K. K. Baral, D. A. Esteves-Macaluso, C. M. Thomas, J. Hellhund, R. Lomsadze, T. W. Gorczyca, C. P. Ballance, et al., Phys. Rev. A **88**,

053402 (2013).

[63] J. P. Connerade, V. K. Dolmatov, and S. T. Manson, J. Phys. B **33**, L275 (2000).

[64] M. Y. Amusia, A. S. Baltenkov, V. K. Dolmatov, S. T. Manson, and A. Z. Msezane, Phys. Rev. A **70**, 023201 (2004).